Table 1 Positional and thermal parameters, selected interatomic distances and average Bi valence for $SrBiO_3$ and $Sr_{0.4}K_{0.6}BiO_3$

	$SrBiO_3$	$Sr_{0.4}K_{0.6}BiO_3$
Space group	$P2_1/n$	$I4/mcm$
Lattice parameters	$a = 5.9480(2)$, $b = 6.0951(2)$, $c = 8.4854(3)$ Å, $\beta = 90.063(6)°$	$a = 5.9416(2)$ Å, $c = 8.4394(4)$ Å
Sr(K) x, y, z	–0.0152(7), 0.5455(4), 0.251(1)	0, 0.5, 0.75
U (Å^2)	0.0078(7)	0.016(1)
Bi1 x, y, z	0, 0, 0	0, 0, 0
U (Å^2)	0.0045(6)	0.0017(5)
Bi2 x, y, z	0, 0, 0.5	–
U (Å^2)	0.0045(6)	–
O1 x, y, z	0.4056(7), 0.4617(7), 0.241(1)	0, 0, 0.25
U (Å^2)	0.019(1)	$U11$, $U33$: 0.033(3), 0.009(2)
O2 x, y, z	0.284(1), 0.190(1), 0.546(1)	0.2219(5), 0.7219(5), 0
U (Å^2)	0.019(2)	$U11$, $U33$: 0.011(1), 0.060(3)
O3 y, y, z	0.187(1), 0.714(1), 0.556(1)	–
U (Å^2)	0.012(2)	–
Rw, χ^2	7.11%, 1.60	8.19%, 1.88
Sr(K)–O (Å)	3.484(6), 2.556(6), 3.618(5) 2.620(5), 3.76(1), 3.01(1), 2.85(1), 2.55(1), 3.03(1), 3.83(1), 2.50(1), 2.83(1)	2.9708(2) × 4, 2.814(2) × 4, 3.150(2) × 4
Bi1–O (Å)	2.28(1) × 2, 2.317(7) × 2, 2.321(6) × 2	2.1098(4) × 2, 2.114(3) × 4
Bi2–O (Å)	2.14(1) × 2, 2.088(7) × 2, 2.123(7) × 2	
v(Bi1)	3.21	4.62
v(Bi2)	4.57	–

U, mean square temperature displacement; R_w, weighted profile agreement factor; v, valence.

distinct distorted octahedral sites. The positional and thermal parameters after the last cycle of refinement, as well as the Bi–O and Sr–O interatomic distances, are given in Table 1. Attempts to refine the cationic or anionic site occupancies did not lead to any deviation from full occupancies. The average Bi–O distances are 2.30(1) and 2.12(1) Å for the two sites. The average valences of Bi1 and Bi2 calculated with the Zachariasen formula[10] and the constants reported previously[11] are +3.21 and +4.57, respectively. As with $BaBiO_3$[9,11], this indicates a partial disporportionation of the Bi cations into Bi^{3+} and Bi^{5+}, which occupy the two distinct crystallographic Bi1 and Bi2 sites. This charge localization is in agreement with the insulating properties of this compound.

The structure of $Sr_{0.4}K_{0.6}BiO_3$ has been refined in the $I4/mcm$ space group (as with $BaPb_{1-x}Bi_xO_3$ in the superconducting region). The main results are reported in Table 1 and a structural model is shown in Fig. 3. The refined K content is 0.56(2), in good agreement with the EDS data. The temperature factors of the oxygen atoms are highly anisotropic with anomalously large components. When refined, the occupancy of the oxygen sites was close to unity. The anomalous values of the temperature factors might reflect a positional disorder of the oxygen atoms depending on whether the neighbouring cations are K or Sr. The Bi cations occupy only one octahedral site with Bi–O distances 2.1098(4) × 2 and 2.114(3) × 4 Å. This yields an average Bi valence of +4.62, which is in good agreement with the value expected from the refined composition (+4.56).

Our preliminary study of the Rb-substituted samples, $Sr_{1-x}Rb_xBiO_3$, shows that these materials, prepared in the same way as the K-substituted ones but using Rb_2O instead of KO_2, exhibit superconductivity with $T_c = 13$ K at $x \approx 0.5$. Owing to the small superconducting volume fraction (~6%) and poor phase purity for Rb-substituted samples, further investigations are necessary to clarify the origin of the superconductivity in this system.

A comparison of the systems $Sr_{1-x}K_xBiO_3$, $BaPb_{1-x}Bi_xO_3$, $Ba_{1-x}K_xBiO_3$ and $BaPb_{1-x}Sb_xO_3$ (ref. 12), with maximum T_c values of ~12 K, 12 K, 30 K and 3.5 K respectively, has shown that keeping the perovskite B site intact is not the only parameter that provides a high T_c. The octahedral tilt scheme influenced by the size of the A cation is also an important aspect. This new system indicates that, in contrast with the Cu-based superconductors where the two-dimensional character seems necessary for a high T_c, the highest three-dimensional symmetry seems to be the clue for a high T_c in bismuth oxides. □

Received 11 April; accepted 3 September 1997.

1. Sleight, A. W., Gillson, J. L. & Bierstedt, P. E. High-temperature superconductivity in the $BaPb_{1-x}Bi_xO_3$ system. *Solid State Commun.* **17,** 27–28 (1975).
2. Mattheiss, L. R., Gyorgy, E. M. & Johnson, D. W. Superconductivity above 20 K in the Ba-K-Bi-O system. *Phys. Rev. B* **37,** 3745–3746 (1988).
3. Cava, R. J. *et al.* Superconductivity near 30 K without copper: the $Ba_{0.6}K_{0.4}BiO_3$ perovskite. *Nature* **332,** 814–816 (1988).
4. Hinks, D. G. *et al.* Synthesis, structure and superconductivity in the $Ba_{1-x}K_xBiO_{3-y}$ system. *Nature* **333,** 836–838 (1988).
5. Klein, T., Harneit, W., Baril, L. & Escribe-Filippini, C. Pinning and vortex dynamics in superconducting (K,Ba)BiO_3 single crystals. *J. Low Temp. Phys.* **105,** 1067–1073 (1996).
6. Marx, D. T. *et al.* Metastable behavior of the superconducting phase in the $BaPb_{1-x}Bi_xO_3$ system. *Phys. Rev. B* **46,** 1144–1156 (1992).
7. Pei, S. *et al.* Structural phase diagram of the $Ba_{1-x}K_xBiO_3$ system. *Phys. Rev. B* **41,** 4126–4141 (1990).
8. Larson, A. C. & von Dreele, R. B. Report LA-UR-86-748 (Los Alamos Laboratory, Univ. California, 1985).
9. Cox, D. E. & Sleight, A. W. Crystal structure of $Ba_2Bi^{3+}Bi^{5+}O_6$. *Solid State Commun.* **19,** 969–973 (1976).
10. Zachariasen, W. H. & Penneman, R. A. Application of bond length–strength analysis to 5f element fluorides. *J. Less Common Metals* **69,** 369–377 (1980).
11. Chaillout, C. *et al.* Bismuth valence order–disorder study in $BaBiO_3$ by powder neutron diffraction. *Solid State Commun.* **65,** 1363–1369 (1988).
12. Cava, R. J. *et al.* Superconductivity at 3.5 K in $BaPb_{0.75}Sb_{0.25}O_3$: why T_c so low? *Nature* **339,** 291–293 (1989).

Acknowledgements. We thank M. Perroux for his help in the high-pressure experiments. This work was partly supported by the Nato Linkage, a French–Russian network of the French MENSR and the Russian project 'POISK'.

Correspondence and requests for materials should be addressed to C.C. (e-mail: chaillout@polycnrs-gre.fr).

Chemical composition of dissolved organic nitrogen in the ocean

Matthew McCarthy*, Tom Pratum†, John Hedges* & Ronald Benner‡

** School of Oceanography, Box 357940, and † Department of Chemistry, Box 351700, University of Washington, Seattle, Washington 98195-7940, USA*
‡ University of Texas, Marine Science Institute, Port Aransas, Texas 78373, USA

Fixed nitrogen is one of the main limiting nutrients for primary production in the ocean[1–3], where it is biologically available in the form of dissolved inorganic and organic matter. Inorganic nitrogen concentrations are consequently very low in surface waters of temperate ocean gyres, yet fixed nitrogen persists in the form of dissolved organic matter. The small, rapidly cycling organic compounds fundamental to microbial and planktonic growth (such as free amino acids, amines and urea[4,5]) account for only a minor fraction of total dissolved organic nitrogen (DON). In contrast, the vast majority of DON, especially in the deep ocean, resides in the form of nitrogenous substances that are resistant to biological degradation. These substances, which represent an

enormous reservoir of fixed nitrogen, are not readily identified by conventional biochemical techniques, but have been assumed to consist largely of structurally complex macromolecules resulting from the degradation and spontaneous abiotic condensation of biochemical precursors[6]. Here we present ^{15}N NMR measurements that contradict this view. Our results show that most higher-molecular-weight DON in the ocean exists in amide form, rather than as a collection of nitrogen heterocycles that might be indicative of spontaneous condensation products. Because these amides are unlikely to form abiotically, the bulk of the ocean's DON reservoir appears to derive directly from degradation-resistant biomolecules.

Ultrafiltered dissolved organic matter (UDOM) was isolated from four depths (surface to 4,000 m depth) in the central Equatorial Pacific Ocean, and from surface waters along a transect in the oligotrophic central North Pacific gyre. These samples include both biologically active surface waters and less dynamic abyssal waters from ocean regions free of direct terrestrial influence. Samples were isolated using tangential-flow ultrafiltration, a size-based technique that reproducibly isolates 20–30% of total DOM from sea water[7,8]. Retention of total DOM ranged from 19% in the deep Pacific to 38% in surface waters, with atomic C/N ratios of the isolates ranging from 15.6 to 18.4 (Table 1).

UDOM represents the larger size fraction of the operationally defined ($<0.1\,\mu$m) DOM pool, and the degree to which it is compositionally representative of lower-molecular-weight oceanic DOM remains to be fully determined. Continuous enzymatic degradation of large to smaller molecules takes place in the water column, and all dissolved material surviving over longer timescales is likely to be affected by this process. Bulk properties of UDOM, including C/N ratios, stable carbon isotopic ratios, radiocarbon 'ages' and overall amino-acid content, are similar to the same properties for total DOM, and are clearly distinct from those of marine biomass or detrital particles[8–10]. Although it is likely that some compositional differences within molecular weight ranges do exist, the comparisons of C/N ratio and overall amino-acid content suggest that UDOM isolation does not greatly fractionate DOM in terms of major nitrogenous components.

Cross-polarization magic-angle-spinning (CPMAS) techniques in nuclear magnetic resonance spectroscopy of solid samples provide a powerful tool for elucidating structural characteristics of complex natural organic mixtures. However, because the low natural abundance and small magnetogyric ratio of the ^{15}N nucleus results in low sensitivity, ^{15}N CPMAS NMR has usually been used only on isotopically enriched materials[11]. Recently, with the use of higher magnetic fields and long signal averaging times, ^{15}N CPMAS NMR has been successfully applied in studies of natural organic matter in soils[12], coal[13] and marine sedimentary deposits[14]. Here we report application of ^{15}N CPMAS NMR with large DOM samples available using ultrafiltration, providing the first comprehensive view of natural nitrogen forms in this major ocean reservoir.

The ^{15}N CPMAS spectra of UDOM samples isolated from the central Pacific Ocean are characterized by a single well-defined peak centred near 260 p.p.m. (Fig. 1a). Although the peak width at half-maximum of the 260 p.p.m. band is similar in surface samples, the width of the same resonance increases in deep waters. This resonance corresponds mainly to the chemical shift range for amide nitrogen[15]. Comparison with similarly obtained ^{15}N CPMAS spectra of several reference biochemicals (Fig. 1b) confirms the assignment: two of the most common amide-containing biopolymers, protein and chitin, have ^{15}N resonances at 259–261 p.p.m. (Fig. 1b) and cannot be distinguished at the resolution of our solid-state NMR experiment. As well as verifying the chemical shift assignments, the reference spectra demonstrate our ability to observe diverse nitrogen species (amides, amides and heterocyclic nitrogen). Apart from the main peak, no other signals can be unambiguously identified in any sample, indicating that only negligible amounts of more-shielded nitrogen (for example, aliphatic amines and non-acylated amino sugars) or less-shielded nitrogen (for example, heterocyclic or imine) are present.

The chlorophyll maximum sample from 100 m is characterized by the higher overall DOC, the lowest C/N and shifts in ^{15}N stable isotope values indicative of active production[8]. The ^{15}N NMR spectrum of this sample also displays the narrowest and most symmetrical resonance, with a chemical shift (260 p.p.m.), width

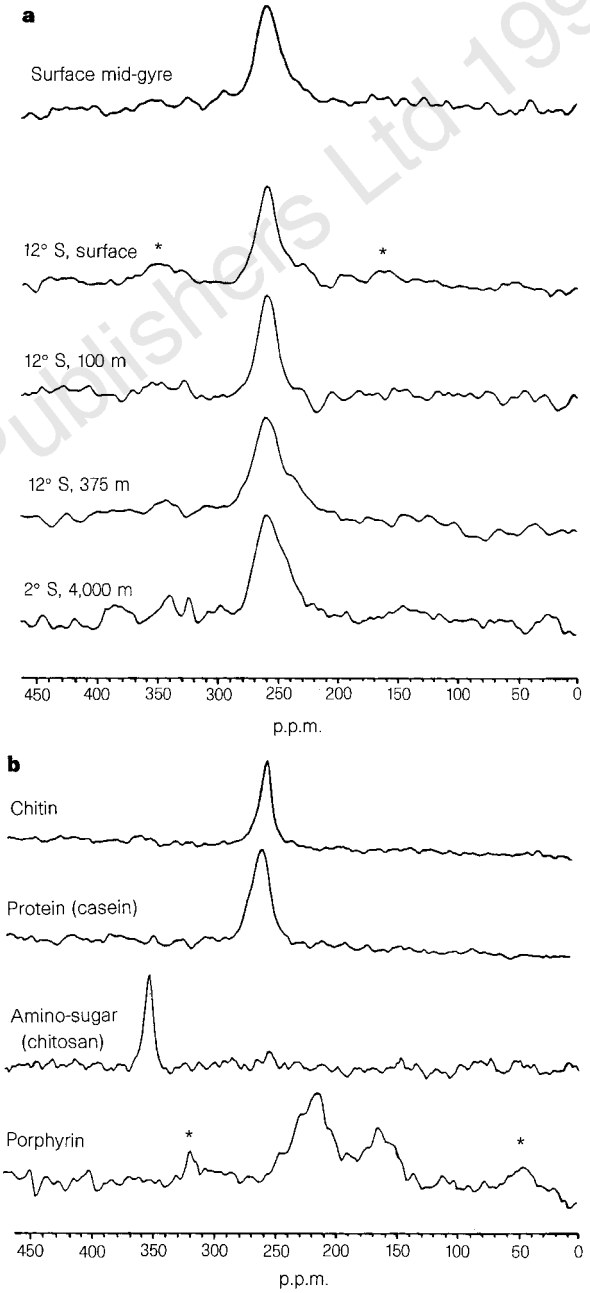

Figure 1 Natural abundance ^{15}N CPMAS spectra for Pacific UDOM samples and selected natural materials. Spinning sidebands (where clearly observable) are indicated by asterisks. **a**, Spectra for Pacific Ocean UDOM samples. The 12° S surface sample was acquired at a slower spin rate of 3.0 kHz, resulting in spinning sidebands for the amide peak. A shortened pulse delay of 500 ms was used to acquire roughly 500,000 transients for the 12° S 375 m and surface samples after replicate analyses of other samples at 500 ms delay resulted only in improved signal-to-noise ratios. **b**, Natural abundance spectra for selected nitrogen-containing biochemicals. Amides: chitin (*N*-acetylglucosamine polymer) and casein (a protein). Amino sugar: chitosan (deacylated chitin). Heterocyclic nitrogen: protoporphyrin IV.

at half-maximum (20 p.p.m.), and range (237–277 p.p.m.) similar to those of the pure amide biopolymers (Fig. 1b). This observation suggests that nearly all UDOM nitrogen at this depth is present as biosynthesized amides.

Because 60–80% of organic nitrogen in biomass or marine particles is recoverable as hydrolysable amino acids[16], peptides might be expected to predominate in UDOM from upper waters. However, only a minor percentage (<10%) of total nitrogen could be recovered from any UDOM isolate as hydrolysable amino acids (Table 1). Furthermore, this fraction of UDOM nitrogen showed little variation with depth, being 8–10% in all samples. The absence of elevated values in surface samples is surprising, indicating that freshly produced UDOM is not greatly enriched in hydrolysable peptide. Similarly low yields have been observed in depth profiles from other ocean basins[9]. The persistance of hydrolysable peptide in the deep ocean suggests that a small fraction of biomass protein—the likely source of this material—is preserved over long timescales. In fact, specific membrane proteins have been found to persist intact in both the surface and deep ocean[17], suggesting that some proteinaceous materials are either difficult to degrade or physically protected from enzymatic hydrolysis.

The unknown amide fraction makes up the majority of total nitrogen in all UDOM samples. This amide could be proteinaceous material which has been rendered largely resistant to conventional hydrolysis methods. However, although there is evidence that acid hydrolysis does not fully account for hydrolysable amino acids in oceanic DOM[18], even a several-fold increase in yield would leave the majority of amide unaccounted for. In addition, the previously noted lack of even a small elevation in amino-acid yield in upper water UDOM does not support the explanation of a proteinaceous material that has become physically protected over time. Curie-point pyrolysis of previous Pacific UDOM samples[19] has also yielded low abundances of amino-acid-derived products. Thus, although some hydrolysis-resistant peptide is likely to be present, other amide forms may also be important components of UDOM nitrogen.

If a substantial portion of the unknown amide is not proteinaceous, the high concentrations and fluxes imply another common and abundant biochemical source. Unusual hydrolysis-resistant amide structures have recently been indicated in some algae[20], but have rarely been reported and are likely to be present only in particulate form. Acetylated amino sugars are the second major amide-containing constituent of biomacromolecules, occurring widely in structural polymers of plants, animals and bacteria[21]. Common marine sources include chitin, a structural component in many eukaryotic plankton species, and bacterial cell wall components, such as mureins and lipopolysaccharides. The potential for long-term preservation of such structural polymers is generally thought to be greater than that for proteins or storage carbohydrates[21], and peptidoglycans in particular contain many uncommon constituents that probably act to deter common hydrolytic enzymes[22]. UDOM from both surface and deep waters is enriched in carbohydrate characterized by low neutral sugar content and constant molecular-level composition[9], suggesting that a similar range of structural polysaccharides may be ubiquitous throughout the oceanic water column[9,23]. Although hydrolysis and quantification of charged sugar residues is difficult[24], pyrolysis of UDOM samples has also indicated *N*-acetyl amino sugar precursors suggestive of structural polymers[19].

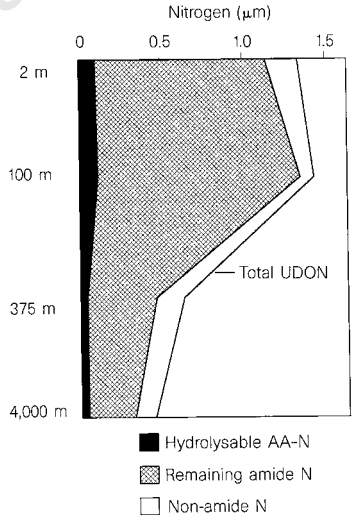

Figure 2 Organic UDOM nitrogen forms in Pacific Ocean. Distribution of the three broad categories of ultrafiltered DON from the depth profile at 12° S, 140° W, and deep-water sample (4,000 m) at 2° S, 140° W in the Pacific Ocean. As described in the text, the differences between amide N and total UDON concentrations are probably made up by stable heterocyclic nitrogen forms (pyrrole/indole-like nitrogen). Note that the depths on the *y*-axis are not to scale.

Table 1 Pacific UDOM recovery and bulk ON composition

	2 m (mid-gyre)	2 m (surface)	100 m (chl. max.)	375 m (O_2 min.)	4,000 m (deep)
DOC (μM)	78	82	85	53	45
% UDOM	30	38	27	19	22
(C/N)	16.4	16.8	15.6	16.9	18.4
UDON (μM)	1.12	1.33	1.42	0.63	0.45
%AA-N	n.d.	8.2	8.2	8.5	9.4
% other amide	75	77	86	66	65
% non-amide	17	15	6	25	26
Centre (p.p.m.)	260	259	261	261	261
Width (p.p.m.)	23	21	20	27	32
Total range (p.p.m.)	217–287	225–285	237–277	206–283	222–280

Total dissolved organic carbon (DOC) values, as well as of carbon-based ultrafiltered dissolved organic matter recoveries (%UDOM), for the central Pacific water samples (12° S, 140° W), including depths corresponding to the oxygen minimum (O_2 min) and chlorophyll maximum (chl. max.). Total UDON concentrations are derived from CHN data, the dry weight recovered and the volume filtered. For UDOM isolates. we give atomic carbon/nitrogen ratios (C/N) and estimates of the contribution made by the three nitrogen classes discussed to total UDON at each depth. Percentage amino-acid nitrogen (%AA-N) is calculated directly from hydrolysable amino-acid data, while the percentage non-amino-acid amide (% other-amide) and the percentage non-amide are derived from integration of the ^{15}N NMR spectra, based on resonance ranges of authentic amide biopolymers. For ^{15}N CPMAS NMR spectra the centre resonance, full width at half maximum and total range at baseline are also given.

Although amide nitrogen clearly dominates all samples, there are also indications of smaller contributions by other nitrogen forms, especially in samples from deep waters with low overall UDOM concentration. Widths of the 260 p.p.m. peak at half maximum, a measure relatively unaffected by baseline noise, clearly increases with water depth (Table 1). The increase is not symmetrical, but instead falls mostly in a small downfield shoulder between 220 and 240 p.p.m. This spectral region is outside the range of authentic amide biopolymers, and corresponds mainly to indole- and pyrrole-like nitrogen[15]. Such heterocyclic structures are among the most stable organic nitrogen forms in the geosphere, accounting for much of the organic nitrogen observed in petroleums[25], coals[13] and some marine sediments[14,25]. Natural marine sources of 'pyrrole-like' nitrogen resonating in the same region include the bases of DNA and RNA (purines and pyrimidines) and the porphyrin backbone of photosynthetic pigments. Although these compounds are present in the ocean at low concentrations, their bases may be relatively stable. In addition to biological sources, it is possible that compounds formed abiotically also contribute. Melanoidins, the complex end-products of sugar and amino-acid condensation, also resonate in this region[26], and their formation has been long hypothesized as an important abiotic pathway for organic matter preservation[27]. Although it is not possible to distinguish specific sources for this signal, the 220–240 p.p.m. shoulder does appear as a consistent feature of all spectra.

Taken together, the ^{15}N NMR, amino acid, and total UDOM nitrogen concentrations in the central Pacific indicate oceanographically consistent depth distributions of three principal nitrogen types throughout the oligotrophic ocean (Table 1, Fig. 2). Although the reactivity of these three classes through the water column seems to be generally similar, the data do suggest some distinct cycling. The downfield shoulder suggests that a small portion of total UDOM nitrogen at all depths is non-amide. This fraction has its highest relative abundance (26%) in the deep ocean, consistent with NMR evidence that it is made up of stable—and thus slowly cycling—heterocyclic nitrogen forms (pyrrole/indole-like nitrogen). Hydrolysable peptide makes up a surprisingly small fraction, accounting for only about 10% of total UDOM nitrogen at all depths. It is the remaining amide component, mainly as a result of its high abundance, that drives almost all of the water-column gradient in UDOM nitrogen. This observation suggests that hydrolysis-resistant peptide or other amide-containing biomolecules may fuel most DON remineralization below the euphotic zone, a process which (coupled with advection) acts to close overall nitrogen budgets in the upper ocean[2].

Despite these gradients, surface-produced amide also constitutes the main component of UDOM nitrogen in the deep Pacific, suggesting that traditional paradigms for DOM cycling in the ocean may need to be re-evaluated. Over 80% of the organic nitrogen in the ocean resides at low concentration in the enormous subsurface reservoir, an environment in which few of the factors commonly understood to control organic matter preservation, such as anoxia, burial or protection by mineral surfaces, can be invoked. This deep-ocean material has overall radiocarbon 'ages' of about 4,000–6,000 years (ref. 28), an observation which has reinforced long-standing hypotheses that condensation reactions produce chemically altered geopolymers which, by virtue of unusual chemical structure, persist over many ocean mixing cycles[6]. Recent work has indicated that specific polysaccharides[9,23] as well as proteins[17] may survive in the ocean over long timescales. However, the wholesale persistence of amide functional groups within the larger-molecular-weight fraction of abyssal DOM indicates that traditional geopolymerization is not a dominant preservation mechanism for this material. In addition, the overall similarities of ^{14}C 'ages', C/N ratios and amino-acid composition between UDOM and total DOM suggest that most organic nitrogen in the ocean retains the principal structural features of the parent biomolecules. Identifying the processes that render common biochemical structures resistant to enzymatic degradation will be central to understanding controls for storage of reduced carbon in the deep sea. □

Methods

Nitrogen-15 CPMAS NMR spectra were obtained on a Bruker AF-300 spectrometer at a frequency of 30.4 MHz and a spin rate of 3.5 kHz. Chemical shifts are referenced to external NO_3^-. Spectral parameters were chosen based on those recently determined as optimum for quantitative ^{15}N solid-state spectra in a variety of natural materials[6,8]. For most spectra, a contact time of 1 ms, an acquisition time of 20 ms and a pulse delay of 1.0 s were used to acquire roughly 250,000 transients. Before Fourier transformation, 125 Hz of line broadening was applied. Neutron activation analysis of a separate Pacific profile (0–4,000 m) indicates that total concentrations of paramagnetic metals in central Pacific UDOM are low (<0.01%) and constant with depth. Amide/non-amide regions were estimates based on resonance ranges of authentic amide biopolymers, and were integrated using Lab-Calc NMR software. The variability of peak integration due to noise is less than 10%, based on integration of equivalent noise regions over the spectral range considered.

Previous work has indicated that optimum acquisition parameters for natural organic mixtures are broad and similar[12,13,29]. Several factors, however, may reduce signal intensities. Although the contact time used might be too short for full cross-polarization of non-protonated N, increasing the contact time could result in attenuation from rotating frame relaxation effects. Quaternary carbon is readily observable in ^{13}C CPMAS UDOM spectra using the same cross-polarization conditions[7,11], and previous studies have indicated that these contact times are adequate for observation of unsaturated heterocyclic nitrogen[13,30]. Nitrogen in asymmetric electronic environments, such as unsaturated or aromatic nitrogen, can also have intensity diverted into spinning sidebands as a result of anisotropic chemical shift effects. The porphyrin in Fig. 1b shows that the unsaturated heterocyclic nitrogens, although observable, are somewhat attenuated by sidebands. Thus, the detection limit for unsaturated heterocyclic nitrogen is likely to be higher than for other nitrogen forms.

Isolation of UDOM using tangential flow ultrafiltration, measurement of total dissolved organic carbon and determination of UDOM recoveries were carried out as described previously[8,9,31]. Total carbon and nitrogen contents of dried samples were measured after vapour-phase acidification with a precision of approximately ±2% using a Carlo Erba 1108 CHN analyser[32]. Hydrolysable amino acids were determined using charge-matched recovery standards after 6 M HCl hydrolysis[16], with individual amino acids quantified as pentafluoropropyl isopropyl esters by gas chromatography with flame ionization detection. Analytical precision for this procedure is ±10% or less for total amino acid yields. The percentage of amino-acid nitrogen (%AA-N) was calculated from the sum of amino-acid nitrogen and the total elemental nitrogen content[16].

Received 7 October 1996; accepted 5 September 1997.

1. Redfield, A. C., Ketchum, B. H. & Richards, F. A. in *The Sea* (ed. Hill, N. H.) 26–76 (Wiley Interscience, New York, 1963).
2. Smith, S. V., Kimmerer, W. J. & Walsh, T. W. Ventrical flux and biogeochemical turnover regulate nutrient limitation of net organic production in the North Pacific Gyre. *Limnol. Oceanogr.* **31,** 161–167 (1986).
3. Jackson, G. A. & Williams, P. M. Importance of dissolved organic nitrogen and phosphorus to biological nutrient cycling. *Deep Sea Res.* **32,** 223–235 (1985).
4. Bronk, D. A. & Glibert, P. M. Nitrogen uptake, dissolved organic nitrogen release, and new production. *Science* **265,** 1843–1852 (1994).
5. Keil, R. G. & Kirchman, D. L. Contribution of dissolved free amino acids and ammonium to the nitrogen requirements of heterotrophic bacterioplankton. *Mar. Ecol. Prog. Ser.* **73,** 1–10 (1991).
6. Harvey, G. R., Boran, D. A., Chesal, L. A. & Tokar, J. M. The structure of marine fulvic and humic acids. *Mar. Chem.* **12,** 119–132 (1983).
7. Benner, R., Pakulski, J. D., McCarthy, M., Hedges, J. I. & Hatcher, P. G. Bulk chemical characteristics of dissolved organic matter in the ocean. *Science* **255,** 1561–1564 (1992).
8. Benner, R., Biddanda, B., Black, B. & McCarthy, M. Abundance, size distribution, and stable carbon and nitrogen isotope compositions of marine organic matter isolated by tangential-flow ultrafiltration. *Mar. Chem.* **57,** 243–263 (1997).
9. McCarthy, M. D., Hedges, J. I. & Benner, R. Major biochemical composition of dissolved high-molecular weight organic matter in seawater. *Mar. Chem.* **55,** 281–297 (1996).
10. McCarthy, M. D., Hedges, J. I. & Benner, R. The chemical composition of dissolved organic matter in seawater. *Chem. Geol.* **107,** 503–507 (1993).
11. Preston, C. M. Applications of NMR to soil organic matter analysis: history and prospects. *Soil Sci.* **161,** 144–166 (1996).
12. Knicker, H., Frund, R. & Ludermann, H. D. The chemical nature of nitrogen in native soil organic matter. *Naturwissenschaften* **80,** 219–221 (1993).
13. Knicker, H., Hatcher, P. G. & Scaroni, A. W. Solid-State 15N NMR spectroscopy of coal. *Energy Fuels* **9,** 999–1102 (1995).
14. Knicker, H., Hatcher, P. G. & Scaroni, A. W. 13C and 15N-NMR spectroscopic investigation on the formation of fossil algal residues. *Org. Geochem.* **6/7,** 661–669 (1996).
15. Levey, G. C. & Lichter, R. L. *Nitrogen-15 NMR Spectroscopy* (Wiley, New York, 1979).
16. Cowie, G. L. & Hedges, J. I. Sources and reactivities of amino acids in a coastal marine environment. *Limnol. Oceanogr.* **37,** 703–724 (1992).
17. Tanoue, E., Nishiyama, S., Kamo, M. & Tsugita, A. Bacterial membranes: possible source of dissolved protein in seawater. *Geochim. Cosmochim. Acta* **59,** 2643–2648 (1995).
18. Keil, R. G. & Kirchman, D. L. Dissolved combined amino acids in marine waters as determined by a vapor-phase hydrolysis method. *Mar. Chem.* **33,** 243–259 (1991).
19. van Heemst, J. D. H., Baas, M., de Leeuw, J. W. & Benner, R. in *Organic Geochemistry* (ed. Oygard, K.) 694–698 (Falch Hurtigtrykk, Oslo, 1993).
20. Derenne, S., Largeau, C. & Taulelle, F. Occurrence of non-hydrolysable amides in the macromolecular constituent of Scendesmus quadricauda cell wall as revealed by 15N NMR: Origin of n-alkylnitriles in pyprolysates of ultralaminae-containing kerogens. *Geochim. Cosmochim. Acta* **57,** 851–857 (1992).
21. De Leuuw, J. W. & Largeau, C. in *Organic Geochemistry* (eds Engle, M. & Macko, S. A.) 23–72 (Plenum, New York, 1993).
22. Rogers, H. J. Peptidoglycans: structure, function and variations. *Ann. New York Acad. Sci.* **235,** 29–51 (1974).
23. Aluwihare, L., Repeta, D. & Chen. R. A major biopolymeric component to dissolved organic carbon in seawater. *Nature* **387,** 166–169 (1997).
24. Bergamaschi, B. A. *The Marine Geochemistry of Carbohydrates: Application and Development of New Techniques of Analysis*, 1–184 (University of Washington, Seattle, 1995).
25. Patience, R. I. *et al.* The functionality of organic nitrogen in some recent sediments from the Peru upwelling region. *Org. Geochem.* **18,** 161–169 (1992).
26. Benzing-Purdie, L., Ripmeester, J. A. & Preston, C. Elucidation of Nitrogen forms in melanoidins and humic acid by nitrogen-15 cross polarization magic angle-spinning nuclear magnetic resonance spectroscopy. *J. Agric. Food Chem.* **31,** 913–915 (1983).
27. Maillard, L. Formation de matieres humiques par action de polypeptides sur les sucres. *C. R. Acad. Sci.* **156,** 148–149 (1912).
28. Williams, P. M. & Druffel, E. R. M. Radiocarbon in dissolved organic matter in the central North Pacific Ocean. *Nature* **330,** 246–248 (1987).
29. Knicker, H. & Ludemann, H. N-15 and C-13 CPMAS and solution NMR studies of N-15 enriched plant material during 600 days of microbial degradation. *Org. Geochem.* **23,** 329–341 (1995).
30. Ripmeester, J. A., Hawkins, R. E., MacPhee, J. A. & Nandi, B. N. On the interaction between pyridine and coal studies by CPMAS ^{15}N NMR. *Fuel* **65,** 740–742 (1986).

31. Benner, R. & Strom, M. A critical evaluation of the analytical blank associated with DOC measurements by high-temperature catalytic oxidation. *Mar. Chem.* **41,** 153–160 (1993).
32. Hedges, J. I. & Stern, J. H. Carbon and nitrogen determinations of carbonate-containing solids. *Limnol. Oceanogr.* **29,** 657–663 (1983).

Acknowledgements. We thank the captain and the crew of the RV *John Vickers* for assistance with obtaining Equatorial Pacific samples, B. Black for help with sample processing, G. Cowie for advice in amino-acid analysis, and D. Bear for guidance and support.

Correspondence should be addressed to M.M. (e-mail: mdmccar@u.washington.edu).

Variability of the North Atlantic thermohaline circulation during the last interglacial period

Jess F. Adkins*§, Edward A. Boyle*, Lloyd Keigwin† & Elsa Cortijo‡

* *Department of Earth Atmosphere and Planetary Sciences, Massachusets Institute of Technology, Cambridge, Massachusetts 02139, USA*
† *Woods Hole Oceanographic Institution, Woods Hole, Massachusetts 02543, USA*
‡ *Centre des Faibles Radioactivitis, Laboratoire mixte CNRS-CEA 91198, Gif-sur-Yvette Cedex, France*

Studies of natural climate variability are essential for evaluating its future evolution. Greenland ice cores suggest that the modern warm period (the Holocene) has been relatively stable for the past 9,000 years[1,2]. Much less is known about other warm interglacial periods, which comprise less than 10% of the climate record during the past 2.5 million years[3–7]. Here we present high-resolution ocean sediment records of surface and deep-water variables from the Bermuda Rise spanning the last interglacial period, about 118,000–127,000 years ago. In general, deep-water chemical changes are coincident with transitions in surface climate at this site. The records do not show any substantial fluctuations relative to the much higher variability observed during the preceding and subsequent cool climates. The relatively stable interglacial period begins and ends with abrupt changes in deep-water flow. We estimate, using ^{230}Th measurements to constrain the chronology, that transitions occur in less than 400 years.

Early results from the GRIP ice core project suggested large climatic changes during the last interglacial[2,8], taken here as roughly equivalent to marine oxygen isotopic stage 5e and the Eemian interglacial on land[9]. Because of structural studies of the ice sheet's bedding[10], comparison with the GISP2 record[1] and studies of the $\delta^{18}O$ of atmospheric oxygen[11], the largest of these apparent climatic instabilities now appear to be artefacts of ice disturbance near the bottom of the core. Nevertheless, the Greenland ice sheet data highlighted how little is known of the climate stability of warm climate periods such as stage 5e, inspiring detailed climate studies on land[6,7] and in marine records[3–5,12,13]. As part of the IMAGES coring program, we raised a 52.7-m-long core (MD95-2036, 33° 41.444′N, 57° 34.548′W, 4,462 m water depth) from the Bermuda Rise, a North Atlantic sediment drift deposit. This core has a continuous record of sedimentation from the Last Glacial Maximum back through the penultimate glaciation (Fig. 1). Visible light reflectance data from the core (a proxy for $\%CaCO_3$) show that we have collected a record that includes all of the major interstadials from 5 to 21 that have been previously identified in Greenland ice cores. Extremely high deposition rates (10–200 cm kyr^{-1}) and penetration through the marine isotope stage 6 provide a unique archive of the ocean's behaviour. As has been previously reported[14], this site is a sensitive indicator of basin scale deep-water chemical variability. Here we present results on the foraminiferal chemistry and ^{230}Th-based clay and carbonate accumulation rates in this core from the depth interval from 42 to 44 m, including marine stages 5e and 5d. To achieve the highest possible temporal resolution, the core was sampled at 1-cm intervals, taking care to avoid extraneous material from burrow structures. Although this sample spacing may seem very fine, it is important to note that bulk density data show that an original depth interval of ~2.4 cm has been compacted to 1 cm.

Several geochemical tracers are used here (Fig. 2). $\delta^{18}O$ measurements of the planktonic foraminiferan *Globigerinoides ruber* reflect a mixture of the global ice volume signature and local surface temperature and salinity conditions. Similarly, benthic $\delta^{18}O$ data reflect deep-water temperatures and the $\delta^{18}O$ value of deep water at this site (determined by global ice volume and deep water hydrography). For the global deep ocean, the $\delta^{18}O$ variation between glacial and interglacial extrema is usually considered to be about two-thirds ice volume and about one-third temperature[15] (although one study argues for a larger role for temperature in the South Atlantic[16]). Cd/Ca ratios were obtained from the benthic foraminiferan *Nutallides umbonifera*. These data reflect the relative mixture of nutrient-depleted source waters of a northern origin (low Cd/Ca) with nutrient-enriched source waters of a southern origin (high Cd/Ca)[14,17,18]. The foraminiferal dissolution index responds to the corrosiveness of bottom waters to $CaCO_3$. Because *Cibicidoides wuellerstorfi* abundance is extremely low in several zones, the benthic $\delta^{13}C$ record is incomplete. These $\delta^{13}C$ data are given in the Supplementary Information, but for deep-water chemical variability we depend instead on the more complete Cd/Ca data[19]. Spectrophotometric reflectance data from the raw sediment were obtained immediately on core splitting[20]; these data are summarized with CIE (Commission Internationale de l'Éclairage) 'L' (lightness) and 'a' (red-to-yellow colour balance) indices. Lightness reflects the relative abundance of white $CaCO_3$ and (typically) darker non-carbonate aluminosilicate material, and the red-to-yellow colour balance reflects the abundance of haematite-rich sediment from the Maritime Provinces of Canada[21,22]. Finally, clay and carbonate fluxes were calculated from $\%CaCO_3$ measurements and from excess ^{230}Th° (where ° stands for decay-corrected) determined, on every other sample, by inductively coupled plasma mass spectrometry (ICP-MS). This calculation is based on the precisely known production rate of ^{230}Th in the water column by dissolved uranium (in flux units of d.p.m. cm^{-2} kyr^{-1}) and the efficient removal of this ^{230}Th to the underlying sediment. On a basin-wide scale, the concentration of ^{230}Th in surface sediments (in units of d.p.m. g^{-1}) is inversely proportional to the total sediment input to the basin (in flux units of g cm^{-2} kyr^{-1}). After accounting for decay since deposition at the surface, down-core accumulation rates of individual sediment components can then be calculated by dividing the ^{230}Th° expected by the concentration measured and multiplying by the component concentration[23–25].

An age model for the interval studied was developed from $\delta^{18}O$ stratigraphy and ^{230}Th-constrained flux variations. Two time control points are taken from the Martinson *et al.*[26] orbitally tuned benthic isotope stack: the beginning of the 5/6 transition (4,380 cm = 131 kyr BP) and the 5d/5e transition (4,280 cm = 114 kyr BP). Previous work at this site established that the sediment composition is a balance between biogenic carbonate (and a small amount of atmospheric dust) falling out of the ocean surface and aluminosilicates from the continental margin transported into the interior of the basin by deep-sea currents[27]. The sedimentation rate at this site is enhanced by lateral sediment focusing, where freshly deposited material is removed from some areas of the seafloor by deep-sea currents and then transported to this site. Low-resolution data from the Holocene[27] and our unpublished studies based on detailed ^{14}C dates at this site for the past 3,000 yr indicate that the basin-wide clay flux and the local focusing factor are correlated, probably linked by seafloor circulation characteristics that control both margin erosion and lateral transport. The ^{230}Th focusing factor

§ Also at MIT/WHOI Joint Program in Oceanography E34-209, Massachusetts Institute of Technology, Cambridge, Massachusetts 02139, USA.